J Solid State Electrochem (2002) 6: 475–484
DOI 10.1007/s10008-001-0253-4

ORIGINAL PAPER

G. Patermarakis · K. Moussoutzanis

Solid surface and field catalysed interface formation of colloidal $Al_2(SO_4)_3$ during Al anodizing affecting the kinetics and mechanism of development and structure of porous oxides

Received: 1 August 2001 / Accepted: 17 September 2001 / Published online: 12 December 2001

Abstract Overall kinetic and potentiometric studies of the growth of porous anodic alumina films in saturated $H_2SO_4 + Al_2(SO_4)_3$ electrolyte showed non-saturation conditions inside the pores and supersaturation conditions at the pore surface/electrolyte interface where the field and the solid surface catalyse the formation of colloidal $Al_2(SO_4)_3$ micelles. Suitable high-strength field thermodynamically sustained electrochemical and chemical kinetic equations were formulated. It was shown that the diameter and surface fraction of charge exchange at the pore bases, the real pore wall surface fraction where oxide dissolution occurs, and its rate are strongly affected by the conditions. The mechanism of growth and structure of the films are quite different from those in H_2SO_4. A mechanism of regular film growth is imposed and the critical current density, above which pitting appears, strongly increases. The formulated theory may predict improved or new Al anodizing technologies.

Keywords Porous anodic alumina · Interface colloidal aluminum sulfate · Field and solid surface catalysis · Kinetics mechanism and structure

Introduction

The structure of uniformly/regularly grown porous anodic alumina films in H_2SO_4 electrolyte is defined by the surface density of the pores, the diameter at their bases and the variation of the diameter along them. The pore surface density, of the order of 10^{10} cm^{-2} [1], depends exclusively on, and decreases with, the current density [1, 2]. The base diameter, up to a few tens of nanometres [1], depends on, and increases with, the temperature and H^+ activity at the pore bases during anodizing [2, 3]. Pores open towards the surface owing to the chemical dissolution of the pore walls by the electrolyte during anodizing [4, 5, 6, 7, 8, 9], similar to open circuit oxide dissolution [5, 6, 7, 8, 9], which is a first-order reaction with respect to H^+ activity and is hindered by incorporated electrolyte anions [3]. At prolonged anodizing a (quasi) maximum limiting thickness appears [4, 10, 11] owing to the opening up of the pores [11, 12]. It increases with current density and decreases with temperature and electrolyte concentration. These films find application for improving the mechanical properties of Al [13], as anticorrosion [4, 10, 14] and decorating [4, 10] coatings and membranes [15], in magnetic memories [16], in catalysis [17, 18, 19, 20, 21, 22, 23], etc.

Low temperatures and electrolyte concentrations and high current densities favour the growth of low-porosity hard films [4, 10]. Sulfate salt additives like $Al_2(SO_4)_3$, $MgSO_4$, Na_2SO_4, $MnSO_4$, $(NH_4)_2SO_4$ and $NiSO_4$ [1, 24, 25, 26, 27] were also considered to favour hard films since, as thought, they reduce the solvent action of the electrolyte. Nevertheless, as shown recently [3], the addition of $Al_2(SO_4)_3$ increases the H^+ activity and therefore the pore base diameter and the concentration of incorporated anions. The rate of pore wall dissolution decreases, showing that the decisive factor is the oxide dissolution, rather than the electrolyte dissolving, ability.

Conditions as above [12, 28] and sulfate additives like $Al_2(SO_4)_3$ and $MgSO_4$ [24], Na_2SO_4 [1], etc, also favour the appearance of pitting, which is due to the non-uniform/abnormal growth of film which thickens excessively at some surface positions [12, 28]. Undesirable non-uniform aspects, thickness, porous structure, porosity, hardness and roughness and cracks appear. The mechanism of pitting appearance and development was recently elucidated [28] and criteria were derived predicting the effect of conditions and additives [28, 29], which showed that hard films and pitting are together

G. Patermarakis (✉) · K. Moussoutzanis
Department of Chemical Engineering,
Section of Materials Science and Engineering,
National Technical University, Iroon Polytechniou 9,
Zografou 157 80, Athens, Greece
E-mail: gpaterma@central.ntua.gr
Tel.: +30-1-7723203
Fax: +30-1-7723184

favoured. Generally, the preparation of regularly grown films with desired (1) low enough porosity or (2) high surface density and base diameter of the pores, thickness and total real surface, are problems so far unsolved.

The above occur if condensed $Al_2(SO_4)_3$ does not form inside the pores. If it forms in the oxide/electrolyte interface, the film growth mechanism and structure may change. As previously shown [3], overall kinetic together with potentiometric studies yield an effective tool to penetrate into the phenomena in the barrier layer and pore walls during anodizing where other experimental analytical methods applied, i.e. to barrier-type films, are ineffective, inaccurate or inapplicable owing to the existence of pores. In this work, by such studies the appearance of condensed $Al_2(SO_4)_3$ during Al anodizing in $H_2SO_4 + Al_2(SO_4)_3$ (saturated) solution and its effect on the mechanism of growth and structure of films are first examined. The possibility to develop methods for solving problems as the above is then discussed.

Experimental

The solubility of $Al_2(SO_4)_3$ in H_2SO_4 was first determined. Solutions of H_2SO_4 (15% w/v or 1.5297 mol dm^{-3}) + $Al_2(SO_4)$ at different concentrations were prepared; steps of 0.1666 mol dm^{-3} were employed around the saturation concentration. They were thermostated at 35 °C and vigorously agitated for 30 min and then left to relax at 25 °C for ~48 h. The lowest concentration where just distinguishable crystals first appeared, 0.75 mol dm^{-3}, was considered the $Al_2(SO_4)_3$ solubility. It was thus determined with an error of ±0.1666 mol dm^{-3}. As verified, it increased with temperature and decreased with the H_2SO_4 concentration.

Al sheets 0.5 mm thick and 99.5% pure were used. The Al composition, the shape and dimensions of the Al anodes and Pb cathodes used and the procedure for the washing and neutralization of Al specimens after anodizing to remove H_2SO_4 from pores and drying are described in detail elsewhere [11]. The washing of the anodized specimens with water and their neutralization with NaOH (0.1 mol dm^{-3}) are performed within a time interval of a few minutes at room temperature [11]. In this case, the washing and neutralization were performed at 35 °C for a relatively long time interval of 10 min in order to remove all the solvable species. Then, the specimens were dried in an air stream and placed in a desiccator for 24 h.

The anodic oxidation was performed galvanostatically in thermostated and vigorously stirred solutions of pure H_2SO_4 (1.5297 mol dm^{-3}) and saturated H_2SO_4 (1.5297 mol dm^{-3}) + $Al_2(SO_4)_3$ (0.75 mol dm^{-3}) at a temperature of 25 °C and current densities of 15, 35, 55, 75, 105 and 135 mA cm^{-2}. The added $Al_2(SO_4)_3$ corresponded to a concentration 0.7666 mol dm^{-3}. It was slightly higher than the saturation concentration. The small amount of precipitate did not appreciably hinder bath stirring while saturated bulk solution was always assured.

When the required anodizing voltage to keep a constant current strongly increased, the process continued up to near 50 V; then it was interrupted. Different times were employed up to those corresponding to ~50 V or near those at which the maximum limiting thickness is attained for slighter voltage variations. As verified, the anodic potential, determined as previously [30], was close to that voltage. For convenience the latter was recorded. The film masses were determined as previously [12]. Then, the films were examined to detect the appearance (or not) of pitting. As previously shown by a detailed examination [28], pitting can be detected by macroscopic observations, optical microscopy, electron microscopy and kinetic criteria, but always the results of macroscopic and optical microscopy examination or of the application of kinetic criteria are sufficient for the sure detection of pitting. For this reason the anodized specimens were examined macroscopically and by an optical microscope as described previously [28] to reveal the appearance (or not) of pitting. In some cases the results were also verified by relevant kinetic criteria [28] (see later).

Results

Dependence of the anodizing voltage on time, film thickness and current density

The anodizing voltage (ΔV) varies with time (t) at different current densities (j) in the cases of $Al_2(SO_4)_3$ concentration ($C_{s,0}$) = 0 and $C_{s,0} = C_{s,s}$ (saturation concentration) as shown in Fig. 1a. Within a t of the order of 1 s, ΔV rises abruptly up to a value depending on j and $C_{s,0}$. Then, during a transient period, ~3–4 min at $C_{s,0} = 0$ and ~1–2.5 min at $C_{s,0} = C_{s,s}$, which decreases with j, ΔV diminishes and a minimum appears (ΔV_m). At $C_{s,0} = 0$ the ΔV versus t plots (Fig. 1a) are given only for the two lower j values since at higher j values intense pitting appeared, not offering any useful information for the subject of this work which concerns mainly the case $C_{s,0} = C_{s,s}$.

At $C_{s,0} = 0$ and $t > t(\Delta V_{min})$, a quasi-steady state is attained and ΔV changes slightly owing to minor changes of solution composition and temperature at the pore bases [28] and their effect on the pore base diameter [3]. At $C_{s,0} = C_{s,s}$ and $t > t(\Delta V_{min})$ the change of ΔV with t strongly alters. At the lowest j, ΔV initially increases with a moderate rate and then strongly increases. At other j values it rises surprisingly abruptly. The film thickness (h) is given from Eq. 1:

$$h = k't = k''jt \quad (t \le t_1) \tag{1}$$

where k'' is a constant (3.09×10^{-6} cm^3 mA^{-1} min^{-1}) and t_1 is the time up to which h increases linearly with t [11]. The time t_1 is identical to, or slightly higher than, t_m at which the maximum average pore diameter near or at the film surface first approaches the cell width and the surface visibly starts to change from a shiny transparent one, similar to Al metal, to a matt milky one [11, 12, 28]. For $t > t_1$, h increases with decreasing rate with t up to t_c, where that rate becomes approximately zero; then the (quasi) maximum limiting h (h_c) is achieved, exceeding slightly or appreciably $k''jt_m$ or $k''jt_1$ [11, 12]. Equation 1 gives the uniform h for regular films and the average h for abnormal films. At $C_{s,0} = 0$ and $j = 15$ and 35 mA cm^{-2}, t_m values are ~110 and ~80 min and the $h(t_m)$ are ~51 and ~86.5 μm (Eq. 1), while the h values at the higher t values employed are < 74.2 and < 108.2 μm, respectively. At $C_{s,0} = C_{s,s}$ and $j = 15$ mA cm^{-2}, $t_m \approx 120$ min. The h values at t_m and the higher t employed are 55.6 and < 69.5 μm. The $h(t_m)$ and h_c increase or decrease together [2, 11, 12]. Then, the h_c must be higher at $C_{s,0} = C_{s,s}$ than at $C_{s,0} = 0$. At all other j values the higher t was $\le t_m$. Using Eq. 1, ΔV versus h [$h \le h(t_m)$] plots were constructed (Fig. 1b), the relative

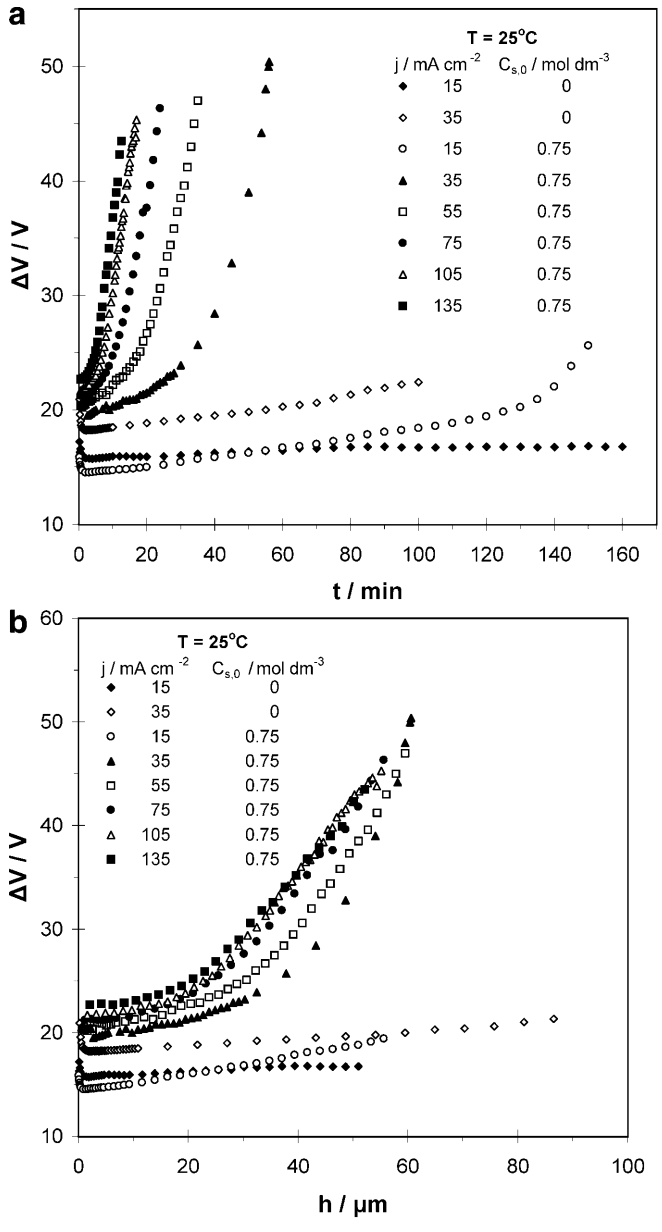

Fig. 1 Variation of the anodizing voltage, ΔV, with (**a**) time, t, and with (**b**) film thickness, h [$h \le h(t_m)$], at $Al_2(SO_4)_3$ concentrations $C_{s,0} = 0$ and $C_{s,0} = C_{s,s}$ and different current densities, j

positions of which differ significantly from those of ΔV versus t plots, especially at high j values.

Variation of film mass with t, h, j and $C_{s,0}$

The plots of the film mass (m) spread over the entire anodized geometric surface area of Al specimens ($S_g = 30.75$ cm^2 [11, 12]) versus t and h [$h \le (t_m)$] are given in Fig. 2a–d. The m versus h plots differ strongly from the m versus t plots and especially their relative positions at different j values.

Overall kinetic models of oxide growth at $C_{s,0} = 0$; conditions of pitting appearance

At $C_{s,0} = 0$ and constant j, when the growth of the film is regular and the diameter of pores at their bases (D_b) remains constant during anodizing, the ΔV versus t plot shows an almost horizontal plateau for $t > t(\Delta V_m)$ (Fig. 1a) [28]. Then, the kinetic model is [12, 28]:

$$A = (kjt - m)\left(4^{-1}\pi S_g d_c k' t\right)^{-1} = A_0 + A_1 t + A_2 t^2 = 4\pi^{-1} p \quad [A_0, A_1, A_2 > 0 \text{ and } t(\Delta V_m) \le t \le t_m] \tag{2}$$

and applies irrespective of the real pore shape [11, 12], where A is a dimensionless factor, k is a constant resulting from Faraday's law, d_c is the density of compact pore wall oxide (3.42 g cm^{-3}) [11], A_0 equals $nD_b{}^2$ where n is the surface density of the pores, A_1 and A_2 are parameters depending on j and the bath temperature (T) and p is the porosity (v/v). Taking into consideration Eq. 1, Eq. 2 becomes:

$$A = A_0 + A_1{}'h + A_2{}'h^2 = 4^{-1}\pi p \quad \{A_0, A_1{}', A_2{}' > 0 \text{ and } h[t(\Delta V_m)] \le h \le h(t_m)\} \tag{3}$$

For $t = 0$ the model of Eq. 2 gives $A_0 = 4\pi^{-1}p$ but initially only a barrier layer exists with zero porosity. Evidently it applies after the t of pore nucleation, which is of the order of 1 s [3], i.e. negligible compared to $t(\Delta V_m) \approx 1$–4 min. The limitation $t(\Delta V_m) \le t \le t_m$ satisfies that condition. The A (or p) parameter is related to basic parameters like n, D_b, etc., and magnifies the m differences, permitting detailed/accurate studies of regular film growth [2, 3, 12].

When a similar ΔV versus t plot plateau and pitting appear, some scatter of points in the A versus t or h plot usually appears and the equations $A = A_0 + A_1 t = A_0 + A_1{}'h$ or Eq. 2 roughly apply (microscopically detected or just macroscopically observed slight pitting) or the equation:

$$A = A_0 + A_1 t + A_2 t^2 + A_3 t^3 \quad (A_0, A_1, A_3 > 0, A_2 < 0, t \le t_m) \tag{4}$$

applies (intense pitting), which anticipates an inverse sigmoid profile [12, 28].

At $C_{s,0} = 0$, the A versus t and h plots obey the models of Eqs. 2 and 3 at 15 mA cm^{-2} and are almost straight lines at 35 mA cm^{-2} (Fig. 3a, c). The A_0, A_1, $A_1{}'$, A_2 and $A_2{}'$ values are given in Table 1. Pitting was not observed in the films at the lower j, but it was just macroscopically observed at the higher j. As j increases, the A versus h plot is shifted down and turned to the right.

The overall kinetic model at $C_{s,0} = C_{s,s}$; conditions of pitting appearance

The A versus t [$t(\Delta V_m) \le t \le t_m$] and h {$h[t(\Delta V_m)] \le h \le h$ (t_m)} plots at $C_{s,0} = C_{s,s}$ are shown in Fig. 3a–d, which

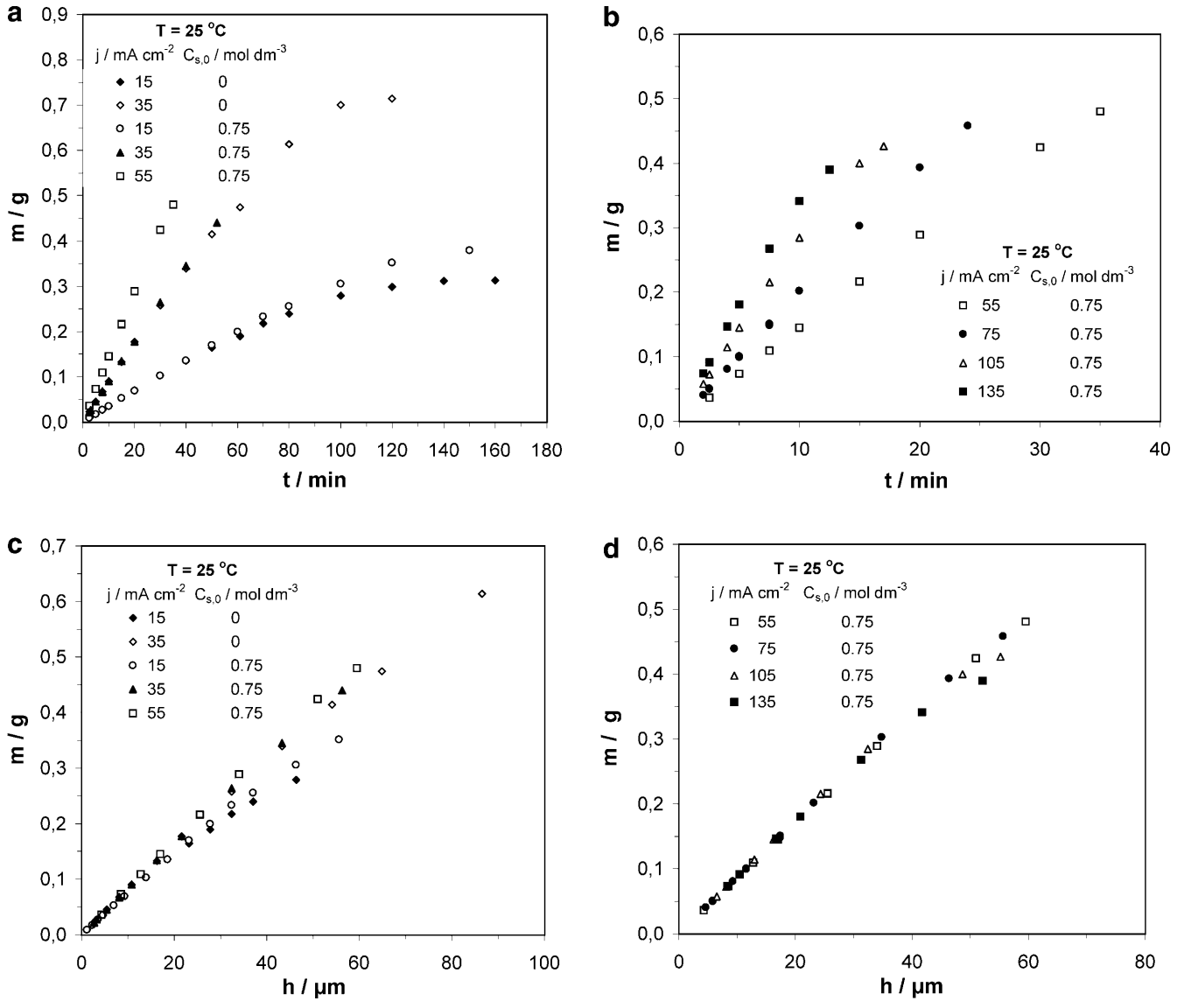

Fig. 2 Variation of the film mass, m, spread over the entire anodized geometric surface area of the Al specimens (30.75 cm^2) with (**a** and **b**) time, t, and with (**c** and **d**) film thickness, h [$h \le h(t_m)$], at $Al_2(SO_4)_3$ concentrations $C_{s,0}=0$ and $C_{s,0}=C_{s,s}$ and different current densities, j. Results at the intermediate $j=55$ mA cm^{-2} appear in all **a**–**d** to help comparisons

differ from those at $C_{s,0}=0$. Some scatter of the points is observed. The equation:

$$A = A_0 + A_1 t + A_2 t^2 = A_0 + A_1' h + A_2' h^2 \qquad (5)$$

satisfactorily applies. From Table 1 it seems that A_0, A_2 and A_2' are >0 while A_1 and A_1' are >0 at low j values and become <0 at $j \ge 55$ mA cm^{-2} where minima appear in the plots.

The A versus h plots yield significant information. Plots are shifted down and turned to the right and the span of A values decreases with j up to ~75 mA cm^{-2}. For higher j values the trends for the plot shift and the span of A variation with j change (Fig. 3d). Appreciable scatter of the points is observed only at $j=15$ and 75 mA cm^{-2}. The span of A variation at $C_{s,0}=C_{s,s}$ is smaller than at $C_{s,0}=0$. At $j=15$ mA cm^{-2} and low h values, A is higher at $C_{s,0}=C_{s,s}$ than at $C_{s,0}=0$. The trend is reversed at higher h values. At $j=35$ mA cm^{-2} the plots originate from almost the same point on the A axis. Then, the plot at $C_{s,0}=C_{s,s}$ is shifted well below that at $C_{s,0}=0$, showing lower p. The shift of the A versus h plot at $C_{s,0}=C_{s,s}$ below that at $C_{s,0}=0$ must be enlarged as j further increases up to ~75 mA cm^{-2}, although for $h \to 0$ the A values may be still close. Irrespective of the n and D_b values, the total real surface of the h_c thickness films increases with h_c [21]. Since h_c is higher at $C_{s,0}=C_{s,s}$, these films must have a higher total real surface than at $C_{s,0}=0$.

At $C_{s,0}=C_{s,s}$, pitting was observed microscopically or just macroscopically at $j \ge 75$ mA cm^{-2}. The characteristic A versus t or h plot does not predict pitting, unlike the case $C_{s,0}=0$ [12, 28]. At $C_{s,0}=C_{s,s}$ a j value lower but near 75 mA cm^{-2} is the critical one (j_c) above which pitting appears. It is also the j boundary where the trend

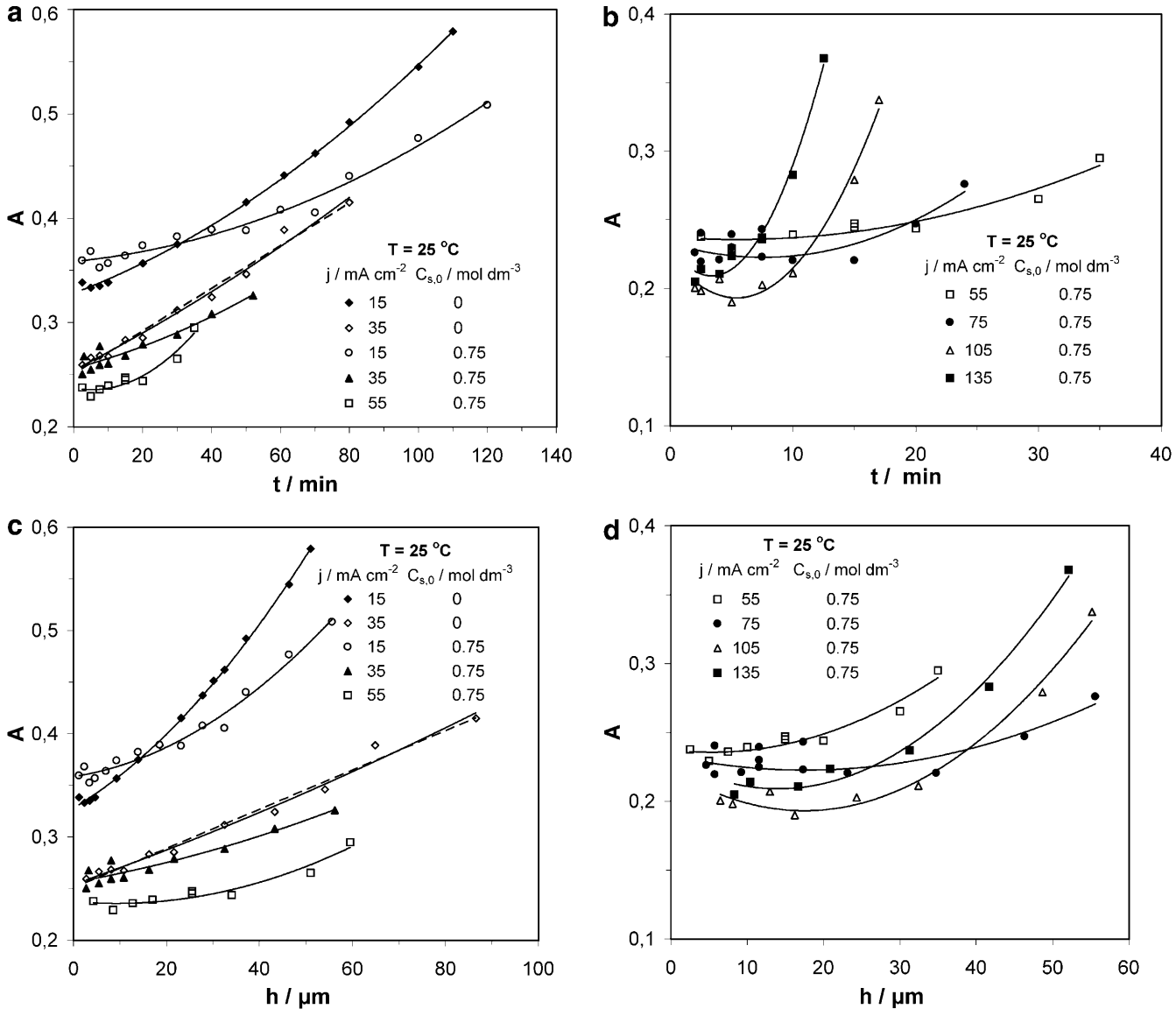

Fig. 3 Variation of the dimensionless factor A with (**a** and **b**) time, t $[t(\Delta V_m) \le t \le t_m]$, and with (**c** and **d**) film thickness, h $\{h[t(\Delta V_m)] \le h \le h(t_m)\}$, at $Al_2(SO_4)_3$ concentrations $C_{s,0} = 0$ and $C_{s,0} = C_{s,s}$ and different current densities, j. Results at the intermediate $j = 55$ mA cm^{-2} appear in all **a**–**d** to help comparisons

of the A versus h plot shift with j changes. In this case, j_c is predicted by the change of that trend. Citation of photographic/microphotographic material of pitted surfaces in both cases, $C_{s,0} = C_{s,s}$ and $C_{s,0} = 0$, was judged to be unnecessary. They were generally similar to those given elsewhere [12, 28] and would add no new information.

Discussion

The necessity for the adoption of D_b variation during anodizing, of non-saturation conditions inside the pores and the formation of colloidal $Al_2(SO_4)_3$ micelles on the pore base and pore wall surfaces at $C_{s,0} = C_{s,s}$ catalysed by the field and solid surface

For regular films, constant D_b and a zero rate of pore wall oxide dissolution, the A versus t or h plot should be a straight line parallel to the t or h axis. When this rate is > 0 the plot obeys Eq. 2 or 3. That rate may become much lower at $C_{s,0} = C_{s,s}$ than at $C_{s,0} = 0$, but not zero.

The profiles and positions of the plots at $C_{s,0} = C_{s,s}$ can be explained only if it is adopted that:

1. The average rate of pore wall dissolution at each h is much lower than that at $C_{s,0} = 0$. Considering a constant temperature inside the pores and equal to T, that rate decreases with j.
2. The D_b decreases with t or h and, for the temperature as above, with j. Then, $A_0 = nD_b^2$ where D_b is the pore base diameter when $t \to 0$ or approximately at $t = t(\Delta V_m)$.

   The average field strength E across the barrier layer is the ratio of the potential drop across the barrier layer

Table 1 Values of the parameters A_0, A_1, A_2, A_1' and A_2' and of the correlation coefficient, COR, derived from fitting Eqs. 2 and 3, $C_{s,0}=0$, and Eq. 5, $C_{s,0}=C_{s,s}$, to the experimental results. In the case $j=35$ mA cm^{-2} and $C_{s,0}=0$ the linear model $A=A_0+A_1t=A_0+A_1'h$ was also applied

J (mA cm^{-2})	$C_{s,0}$ (mol dm^{-3})	10^4A_0	10^4A_1 (min^{-1})	10^6A_2 (min^{-2})	$10^4A_1'$ (min^{-1})	$10^6A_2'$ (min^{-2})	COR
15	0	3270	13.64	8.43	29.45	39.17	0.9986
35	0	2539	17.26	4.41	15.96	3.77	0.9929
35	0	2504	20.64	0	19.08	0	0.9919
15	0.75	3585	3.16	7.95	6.81	37.00	0.9893
35	0.75	2559	8.66	9.48	8.01	8.11	0.9590
55	0.75	2374	–6.67	61.80	–3.92	21.40	0.9669
75	0.75	2330	–27.16	178.61	–11.72	33.26	0.8708
105	0.75	2228	–110.34	1023.29	–34.01	97.21	0.9912
135	0.75	2301	–124.79	1851.57	–29.91	106.40	0.9939

($\Delta P_{b,l}$), which is $\sim\Delta V$, to the thickness of the barrier layer [$2^{-1}(D_c–D_b)$] where D_c is the cell width [3]. Therefore, E is given by the equation:

$$E = \Delta P_{b,l}\left[2^{-1}(D_c - D_b)\right]^{-1} \approx \Delta V\left[2^{-1}(D_c - D_b)\right]^{-1} = n^{1/2}\Delta V\left[2^{-1}\left(n^{1/2}D_c - n^{1/2}D_b\right)\right]^{-1} \quad (6)$$

The anodizing ratio [$E^{-1} \approx 2^{-1}(D_c–D_b)/\Delta V$] for sulfate electrolytes generally varies from 0.8 to 1.4 nm V^{-1} [9, 10], with a mean value of $\sim$1.1 nm V^{-1} [11]. E varies from 1.25×10^7 to 7.14×10^6 V cm^{-1} with a mean value $\sim9.09\times10^6$ V cm^{-1}. Since E decreases with D_b [3], it could be assumed that the increase of ΔV with t or h [$t > t(\Delta V_m)$] is solely due to the decrease of D_b. Figure 1 shows that ΔV can exceed 50 V. Using $nD_c^2 = 4/3$ [30] and n values from the literature [1, 9, 10, 22] and adopting that, as ΔV becomes $\gg$ 50 V, $nD_b^2 \to 0$, Eq. 6 gives unacceptable E values ($> 10^8$ or even 10^9 V cm^{-1}). The increase of ΔV is not justified solely by the decrease of D_b.

Then, it could be assumed that a part of $\Delta P_{b,l}$ is the potential drop across the barrier layer. The remainder is that across a precipitate layer covering the pore base surface. However, since the $Al_2(SO_4)_3$ concentration inside the pores increases towards their bases [28, 29, 31], this precipitate layer should become thicker as h increases, gradually filling the pores from their bases towards their mouths. The anodizing process should be strongly retarded and early on it should cease to take place. However, in actual fact the anodizing process continues to take place regularly. Another explanation must be valid. Its basic suggestions, together with points (1) and (2) above, are:

3. At high $C_{s,0}$ values the H_2SO_4 and $Al_2(SO_4)_3$ concentrations inside the pores slightly increase towards the pore bases and with j [29]. At the pore bases the anodizing temperature (T_a) is $T_a > T$ and $T_a–T$ increases with h and j and decreases with T [11]. The increase of H_2SO_4 concentration and temperature reduces and enlarges respectively the $Al_2(SO_4)_3$ solubility. The effect of temperature predominates and non-saturation conditions exist inside the pores.
4. Supersaturation conditions exist in the double layer on the positively charged (by the field) pore base surface, where the Al^{3+} and SO_4^{2-} concentrations strongly increase towards the surface, and in the attached layer on the pore wall surface which is also positively charged by adsorbed H^+ [3], where the Al^{3+} concentration similarly increases and SO_4^{2-} are attached to the surface [3]. The field and solid surface at the pore bases and the surface on the pore walls catalyse the growth of $Al_2(SO_4)_3$ nuclei and microcrystallites as colloidal micelles (Fig. 4), negatively charged by the anions in excess in the first layer or those attached to the wall surface. They stick on the positively charged surfaces while coagulation is prevented.
5. In surface positions occupied by micelles the processes almost cease. Micelles uptake Al^{3+} from those rejected in the remaining surface at pore bases by the so-called "field assisted" dissolution [1, 4, 10, 25, 26, 27, 32, 33, 34] or on the pore walls by chemical dissolution of oxide. Al^{3+} and anions are successively coordinated. Micelles swell, retaining their charge.
6. Gradually, oxide is consumed even beneath micelles where other nuclei probably appear, pushing micelles away. Large micelles are finally detached, drop in the pore base filling solution and dissolve; other micelles appear and a dynamic equilibrium is thus attained. Fractions θ of the pore base surface and θ_x' of a ring-shaped surface increment ΔS_p on pore walls at a distance x from the film surface (Fig. 4) are occupied by micelles. Al^{3+} and H^+ are rejected at high rates from the pore base surface [3]. The mobile H^+ quickly enter the solution but Al^{3+} remain for long enough time in the double layer and are accumulated. Even the Al^{3+} concentration in the pore base layer seems to exceed that in the wall layer. Hence $\theta > \theta_x'$.
7. The supersaturation conditions in the first layer, and θ, are affected by the field strength on the surface, the $Al_2(SO_4)_3$ and H_2SO_4 concentrations and the temperature at the pore bases, while these conditions in the second layer, and θ_x', are affected by the distri-

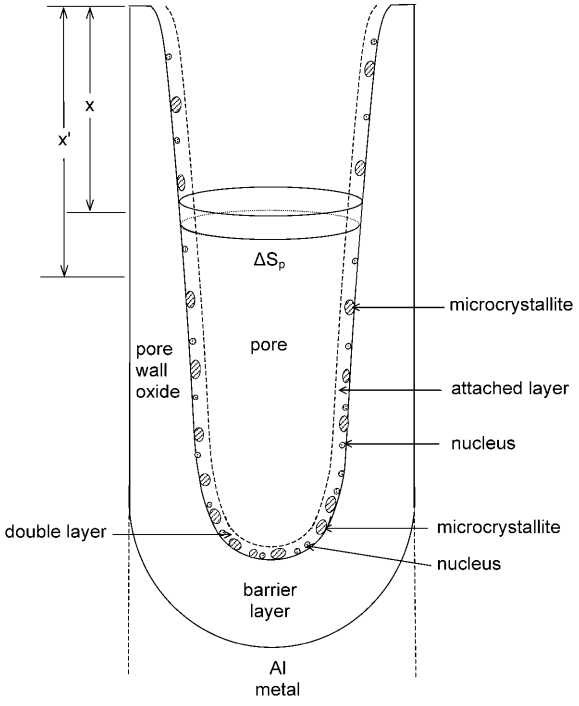

Fig. 4 Schematic representation of the cross section parallel to the pore axis of a cell of oxide where the pore wall oxide, the barrier layer, the pore, a ring-shaped surface increment on the pore surface at a distance x and the inflection point of the pore wall generative at a distance x' from the film surface are shown. The double layer on the pore base surface and the attached layer on the pore wall surface and the formation of $Al_2(SO_4)_3$ nuclei and microcrystallites, micelles, in contact with the surfaces are distinguished

bution of the last three parameters along the pores. The H_2SO_4 concentration seems to exert a minor effect. The main effect is exerted by the other parameters, with intensity decreasing with their order. The $Al_2(SO_4)_3$ concentration enlarges and the temperature reduces both θ and θ_x'.

The high-strength field electrochemical kinetic equations describing the ionic migrations from the pore base surface towards the oxide/metal interface at $C_{s,0} = C_{s,s}$; interpretation of the variation of ΔV and D_b with t, h and j

The oxide formation mechanism embraces the migrations of OH^- and O^{2-} from the pore base surface towards the oxide/Al interface [3], where oxide exclusively forms [30, 35] (Fig. 4). Gradually, OH^- ions decompose to O^{2-} and H^+ which migrate towards the interface and surface. During the normal oxide growth at $t \geq t(\Delta V_m)$ where D_b is almost constant, a steady state for the flux rates of OH^-, O^{2-} and H^+ is attained inside the barrier layer. The flux rates of OH^- and H^+ decrease and that of O^{2-} together with the local field strength increases towards the Al. The field strength in the interface and the real surface of charge exchange at the hemispherical bases of n pores corresponding to 1 cm^2 of geometric surface area of the film, $2^{-1}\pi n D_b^2$, vary oppositely. The true ionic current densities of O^{2-} and OH^- leaving the surface, $j_{OH^-,t}$ and $j_{O^{2-},t}$, are the ratios of the corresponding ionic current densities per cm^2 of the geometric surface area of the film, j_{OH^-} and $j_{O^{2-}}$ correspondingly, to the above real surface of charge exchange at the bases of the n pores. As previously shown by a detailed theoretical analysis [3], these true ionic current densities are given by the equations:

$$j_{OH^-,t} = jF_c^{-1}[(\pi n D_b^2)^{-1} - (\pi n D_c^2)^{-1}] \tag{7}$$

$$j_{O^{2-},t} = 2jF_c^{-1}(\pi n D_c^2)^{-1} \tag{8}$$

and obey the high-strength field equations [3]:

$$\begin{aligned} j_{OH^-,t} &= jF_c^{-1}\left[(\pi n D_b^2)^{-1} - (\pi n D_c^2)^{-1}\right] \\ &= B_1 \exp[(-W_1 N + n_1 a_1 F_c E_b)/(RT_a)] \\ &\quad \times \left(k_w a_{H^+,b}^{-1} + b\right) \end{aligned} \tag{9}$$

$$\begin{aligned} j_{O^{2-},t} &= 2jF_c^{-1}(\pi n D_c^2)^{-1} \\ &= B_2 \exp[(-W_2 N + n_2 a_2 F_c E_b)/(RT_a)] \end{aligned} \tag{10}$$

where F_c is Faraday's constant, B_1 is a variable (see later), B_2 is a constant, W_1 and W_2 are the activation energies for OH^- and O^{2-} migrations, n_1 and n_2 are the valences of OH^- and O^{2-}, a_1 and a_2 are the half-jump (activation) distances, N is the Avogadro constant, R is the universal gas constant, T_a is in K, E_b is the field strength on the pore base surface, $a_{H^+,b}$ is the activity of H^+ at the pore bases which is close to that in solution, a_{H^+}, as are the relevant H^+ concentrations also [3, 28, 29, 31], k_w is the ionic product of H_2O and b is a parameter increasing with E_b and decreasing with T_a. The $-W_1N + n_1a_1F_cE_b$ and $-W_2N + n_2a_2F_cE_b$ are < 0.

B_1 equals $B_1'K$, where B_1' is a constant and K is the equilibrium constant of the process Al^{3+}(bare sites) $+ OH^-_{(b/d)} \leftrightarrows Al^{3+}OH^-$ taking place on the surface. The index b/d means the barrier layer/double layer interface. When $E_b = 0$, K obeys the equation $\Delta G = \Delta G° + RT_a \ln K = \Delta H° - T_a \Delta S° + RT_a \ln K = 0$, where ΔG is the Gibbs energy and $\Delta G°$, $\Delta H°$ and $\Delta S°$ are the standard Gibbs energy, enthalpy and entropy, i.e. $K = \exp(\Delta S°/R)\exp[-\Delta H°/(RT_a)]$. For $E_b \neq 0$ it is transformed to $K = \exp(\Delta S°/R)\exp[(-\Delta H° + 2n_1a_1'F_cE_b)/(RT_a)]$, where a_1' is the half-jump distance of OH^- transfer from the surface of the double layer to a coordinated site of the oxide surface. Hence $B_1 = B_1''\exp[(-\Delta H° + 2n_1a_1'F_cE_b)/(RT_a)]$, where $B_1'' = B_1'\exp(\Delta S°/R)$, i.e. a constant.

When $Al_2(SO_4)_3$ micelles form on the pore base surface, the real surface of charge exchange at the hemispherical bases of n pores is $2^{-1}\pi(1-\theta)nD_b^2$. Then, it is easily conceived that the real ionic current densities $j'_{OH^-,t}$ and $j'_{OH^{2-},t}$ given by Eqs. 7 and 8 in this case become:

$$j_{OH^-,t}{}' = (1-\theta)^{-1} j_{OH^-,t} = (1-\theta)^{-1} jF_c^{-1}\left[\left(\pi n D_b^2\right)^{-1} - \left(\pi n D_c^2\right)^{-1}\right] \quad (11)$$

$$j_{O^{2-},t}{}' = (1-\theta)^{-1} j_{O^{2-},t} = (1-\theta)^{-1} 2jF_c^{-1}(\pi n D_c^2)^{-1} \quad (12)$$

As for the case of no formation of micelles in the pore base surface ($\theta = 0$), these real ionic current densities must obey the high-strength field equations:

$$j_{OH^-,t}{}' = (1-\theta)^{-1}\left[\left(nD_b^2\right)^{-1} - \left(nD_c^2\right)^{-1}\right] = j^{-1}\pi B_1''\{\exp[(-\Delta H^\circ - W_1 N + \left(2n_1 a_1' + n_1 a_1\right)F_c E_b)/(RT_a)]\}\left(k_W a_{H^+,b}^{-1} + b\right) \quad (13)$$

$$j_{O^{2-},t}{}' = [(1-\theta)nD_c^2)]^{-1} = 2^{-1} j^{-1}\pi B_2 \exp[(-W_2 N + n_2 a_2 F_c E_b)/(RT_a)] \quad (14)$$

At constant T_a, E_b increases with j and θ (Eq. 14). The formation of micelles is indeed field catalysed, verifying suggestions (4) and (6). The suitable combination of Eqs. 13 and 14 gives:

$$\left(nD_b^2\right)^{-1}\left(nD_c^2\right) = 1 + 2B_1'' B_2^{-1} \times\{\exp[(-\Delta H^\circ - W_1 N + W_2 N + \left(2n_1 a_1' + n_1 a_1 - n_2 a_2\right)F_c E_b)/(RT_a)]\} \times\left(k_W a_{H^+,b}^{-1} + b\right) \quad (15)$$

The sign of $-\Delta H^\circ - W_1 N + W_2 N + (2n_1 a_1' + n_1 a_1 - n_2 a_2)F_c E_b$ is unknown. It seems that, irrespective of this sign, for small T_a and E_b changes the exponential term varies imperceptibly, opposite to b which varies appreciably. At constant T_a and $a_{H^+,b}$, E_b and D_b vary oppositely. At constant $a_{H^+,b}$ and E_b, T_a and D_b vary similarly. At constant $a_{H^+,b}$ and D_b, T_a and E_b vary oppositely.

Constant $T_a = T$ is considered. The concentrations of $Al_2(SO_4)_3$ at the pore bases and of Al^{3+} and SO_4^{2-} in the double layer increase with h [28, 29, 31], enlarging the number and sizes of micelles and θ which, in turn, increases E_b and reduces D_b, verifying suggestion (2). The changes of local field strength across the barrier layer and in the oxide/Al interface with the real free surface predict similar variations of E and θ. Then, from Eq. 6, ΔV increases.

At each h the $Al_2(SO_4)_3$ concentration at the pore bases, and θ, increase with j. The E_b and b increase and D_b decreases with both θ and j. Both n and D_b decrease, verifying suggestion (2). The $nD_b{}^2$ diminish and both D_c and D_c–D_b increase. The variation of local field strength across the barrier layer shows that E and therefore ΔV increase monotonically with j.

T_a actually rises with both h and j, causing some increase of D_b, reduction of θ and E_b and finally some reduction of ΔV. The rise of T_a competes with the effects of h and j "per se" and finally the ΔV versus h plots and their relative positions at different j values are those shown in Fig. 1b.

The kinetics of pore wall chemical dissolution at $C_{s,0} = C_{s,s}$; interpretation of its strongly lower rate when compared to that at $C_{s,0} = 0$

When no $Al_2(SO_4)_3$ micelles form, as previously shown by a detailed experimental and theoretical analysis [3], the average local rate of pore wall oxide dissolution ($r_{d,x}$, length/time) in the surface ΔS_p at the position x (Fig. 4) obeys:

$$r_{d,x} = k_{d,x} a_{H^+,x} \approx k_{d,x} a_{H^+} \quad (16)$$

where $a_{H^+,x}$ is the activity of H^+ in the pore filling solution near that position, which is $\sim a_{H^+}$ [28, 29, 31], and $k_{d,x}$ is the local rate constant which depends mainly on the concentration of incorporated anions in a thin surface oxide layer and decreases with it [3]. Then:

$$r_{d,x} = k_{d,x} a_{H^+,x} = dz/dt = (\Delta S_p)^{-1}(\Delta S_p dz/dt) = (\Delta S_p)^{-1}(dv/dt) \quad (17)$$

where z is the thickness of the pore wall oxide and v is the volume of dissolved oxide. The average $r_{d,x}$ along the pores of a film of thickness h is $r_{d,a,h} = k_{d,a,h} a_{H^+,a,h} \approx k_{d,a,h} a_{H^+}$, where $k_{d,a,h}$ and $a_{H^+,a,h}$ are the corresponding average $k_{d,x}$ and $a_{H^+,x}$. For constant D_b, as at $C_{s,0} = 0$, the variation of $r_{d,a,h}$ with h is determined by a specific method [3, 36] based on suitable treatment of Eqs. 2 and 3. At $C_{s,0} = C_{s,s}$, D_b varies and it cannot be accurately applied, mainly at high j values. The very low $r_{d,a,h}$ values at $C_{s,0} = C_{s,s}$ are explained by the following method. In the ΔS_p surface, oxide dissolves almost solely in the $(1-\theta_x')\Delta S_p$ free surface and the mean local rate, $r_{d,x}'$, is:

$$r_{d,x}{}' = (1-\theta_x{}')\Delta S_p(dz/dt)\left(\Delta S_p\right)^{-1} = (1-\theta_x{}')(dz/dt) = (1-\theta_x{}')k_{d,x} a_{H^+,x} \quad (18)$$

The $r_{d,x}'$ and the mean value, $r_{d,a,h}'$, decrease with θ_x' and the mean θ_x', $\theta_{a,h}'$.

The distributions of electrolyte anions across the barrier layer and pore walls around the pore bases are identical. Their local concentration decreases from the surface to the interface and cell boundaries prior to, or at, which it is minimized. For constant H_2SO_4 concentration, T and j and invariable D_b with h, their surface concentration increases with their concentration and the ratio of Al^{3+} concentration to that of H^+ in the bath and with D_b [3, 36]. Their concentration on the surface and inside the oxide and the depth of their penetration increase with $C_{s,0}$ and up to that where micelles do not

form. For higher $C_{s,0}$ values, micelles form, θ increases, D_b decreases and these concentrations and depth decrease with $C_{s,0}$, increasing $k_{d,x}$. Simultaneously, θ_x' increases with $C_{s,0}$, reducing $r_{d,x}'$. On approaching $C_{s,s}$ the effect of θ_x' becomes much more significant than that of $k_{d,x}$, justifying the strongly lower $r_{d,x}'$ and $r_{d,a,h}'$ at $C_{s,0} = C_{s,s}$. At each h, the $Al_2(SO_4)_3$ concentration at every position x inside the pores and θ_x' increase with j [29] and the $r_{d,x}'$ and $r_{d,a,h}'$ are reduced, verifying suggestion (1).

The above chemical and the previous electrochemical kinetics are consistent with suggestions (1)–(7), validating the employed methodology for the whole above analysis.

Mechanism of porous layer growth at $C_{s,0} = C_{s,s}$; justification of the A versus t or h plots

At $C_{s,0} = 0$, D_b remains almost constant. The composition of the pore filling solution is close to that of bath [31]. For cylindrical pores ($r_{d,x} = 0$) the distribution of anions across the barrier layer is identical to that everywhere on the pore walls. The same is valid for the variation of $k_{d,x}$, which increases from the surface towards the oxide/Al interface and cell boundaries.

However, $r_{d,x} > 0$ and the time inside which oxide dissolves at a position x, $(h–x)k'^{-1}$, and therefore the pore diameter, increase towards the pore mouths. The variation of $k_{d,x}$ across the pore walls predicts an accelerated increase of diameter at each position. The real pore shape then must be that of an elongated trumpet, to which the A (or p) versus t or h plots agree.

At $C_{s,0} = C_{s,s}$ the pores also open towards their mouths, but D_b decreases, the surface concentration of incorporated anions in the pore bases region may decrease and their distribution across the oxide may vary with h [36]. Irrespective of some influences of these changes, the pore wall surface generative must have a sigmoid profile with an inflection point at a distance x' from the surface, beyond which pores open towards their mouths like an elongated trumpet and close to the bases like an elongated half-barrel. The x' increases with h.

For constant T_a ($= T$), the reduction of D_b with h and j and the increase of diameter at each position and of x' with t or h at $C_{s,0} = C_{s,s}$ easily justify the A (or p) versus h plot profiles (Fig. 3c, d) and the minima at intermediate and high j values. The above enlargement of the pores is on average much smaller than at $C_{s,0} = 0$ since, at each h, $r_{d,x}' < r_{d,x}$ and $r_{d,a,h}' < r_{d,a,h}$. If θ_x' and $\theta_{a,h}'$ are not high enough (or $r_{d,x}'$ and $r_{d,a,h}'$ are not small enough) the A versus h plots may resemble those of Eqs. 2 or 3, as at low j values (≤35 mA cm^{-2}). Finally, the linear dependence of $\ln n$ on $\ln j$ [2], the effect of h and j on the $Al_2(SO_4)_3$ concentration distribution inside the pores and on θ, D_b, θ_x', $\theta_{a,h}'$, $r_{d,x}'$ and $r_{d,a,h}'$ and the rise of T_a and of the temperature at each x position with h, j and x [11], which affects oppositely these parameters, explain the relative plot positions.

Establishment of a self-controlling mechanism of regular oxide growth at $C_{s,0} = C_{s,s}$

If $Al_2(SO_4)_3$ micelles do not appear at the pore bases, pitting develops in conditions where $\partial a_{H^+,b}/\partial j > 0$ ($h \to 0$) [28, 29]. At each triad of T, H_2SO_4 concentration ($C_{a,0}$) and $C_{s,0}$ there is a critical j_c above which $\partial a_{H^+,b}/\partial j > 0$, which increases with T and $C_{a,0}$ and decreases with $C_{s,0}$. At the employed T, $C_{a,0}$ and $C_{s,0} = 0$, $j_c \approx 25$ mA cm^{-2} [28], to which the appearance of pitting at 35 mA cm^{-2} agrees. Pitting develops like an avalanche phenomenon at the early stages of the process, mainly in surface regions where heat abduction is more effective [28], as a result of an accelerated increase of local j and h. A quasi-steady state is then attained as regards the distribution of local j on the surface; the local h increases faster at these positions where finally oxide excessively thickens.

When $Al_2(SO_4)_3$ micelles form, assuming that the conditions instantaneously favour the appearance of pitting at a position, the increase of local j and h will increase θ, reduce D_b and increase the necessary ΔV. The ionic current through the barrier layer at these positions is strongly retarded. A self-controlling mechanism for uniform oxide growth is thus established.

If T_a were equal to T or T_a–T were negligible, pitting would not appear or j_c would be enormously higher. The strong increase of ΔV with t gives rise to T_a. The increase of T_a favours the regular growth of film [28, 29] but, simultaneously, it also hinders the formation of micelles, facilitates their removal and dissolution and renders the mechanism of the regular growth of film less effective. As a result of this T_a increase, the j_c at $C_{s,0} = C_{s,s}$ finally becomes only ~3 times higher than the j_c at $C_{s,0} = 0$.

When micelles do not form, $Al_2(SO_4)_3$ and other sulfate additives favour pitting appearance at $C_{s,0} < C_{s,s}$ [1, 24, 29] since their presence reduces j_c [29]. However, at $C_{s,0} = C_{s,s}$, j_c becomes much higher by the above mechanism. Micelles may form, mainly on the pore base surface, also at $C_{s,0}$ lower, but not largely different, than $C_{s,s}$, exerting similar but lighter effects. Hence, j_c initially decreases with $C_{s,0}$, is minimized near $C_{s,s}$ and then abruptly rises.

Even at $C_{s,0} \ll C_{s,s}$, conditions retarding the transport of Al^{3+} and SO_4^{2-} inside the pores or reducing the $Al_2(SO_4)_3$ solubility may cause the formation of micelles, mainly on the pore base surface. This may occur even at $C_{s,0} = 0$ in severe conditions, i.e. very low T values. These explain the required significant increase of ΔV with t at $C_{s,0} = 0$, moderate T values, moderate or high j values and high h values, i.e. many tens of micrometres [30], where the transport of ions inside the pores is retarded. The formation of micelles may be necessary for each electrolyte to obtain films with very low porosity.

The strong increase of ΔV with t, the change of the trend of the A versus t or h plot shift at $j > j_c$ and the turn to the left (Fig. 3) imply significant T_a–T values, probably several degrees centigrade. A method of keeping T_a–T low enough would make the above mechanism more effective, and would reinforce the p differences between $C_{s,0} = C_{s,s}$ and $C_{s,0} = 0$, etc. Precise measurements of T_a by some method may give much additional information. Further investigation is necessary for the complete elucidation of these phenomena which, nevertheless, are very promising.

Conclusions

From the results of this study the following concluding remarks can be drawn:

1. During Al anodizing in $H_2SO_4 + Al_2(SO_4)_3$ (saturated) solution, colloidal $Al_2(SO_4)_3$ micelles form on the pore surface, catalysed by the field and solid surface, strongly affecting the kinetics and mechanism of film growth by reducing the surface fraction of charge exchange and diameter at the pore bases and the real fraction of the wall surface where oxide dissolves.
2. At each condition there is a specific current density above which films have lower porosity at each h than those in pure H_2SO_4 solution. At each of these j values there is a specific thickness where the porosity becomes a minimum. Higher h_c thickness films are also obtained.
3. A self-controlling mechanism for regular/uniform film growth is established. The critical j_c, above which pitting appears, becomes much higher than in H_2SO_4. At $j = j_c$ the porosity is less variable with h and on average the least.
4. The method may be improved by controlling T_a so that T_a–T remains low enough. Although the necessary anodizing voltage will rise, the product films will have improved features.
5. The use of saturated or dense solutions together with severe/extreme conditions, i.e. very low temperatures, high current densities, etc., may improve the already employed technologies for Al anodizing, or may be developed for important new ones.
6. Interventions by suitable methods in the elementary steps of processes at pore bases and on pore walls controlling the mechanism of film growth are possible. Hopeful prospects to surpass different problems of Al anodizing by such methods now appear. This is of great importance for the theory and practice of Al anodizing and the applications of films.
7. The results of this study may have a broader significance for the electrochemistry in dense solutions and severe/extreme conditions.

References

1. Wood GC, O' Sullivan JP (1970) Electrochim Acta 15:1865
2. Patermarakis G, Moussoutzanis K (1995) J Electrochem Soc 142:737
3. Patermarakis G, Moussoutzanis K, Chandrinos J (2001) J Solid State Electrochem (in press)
4. Diggle JW, Downie TC, Goulding CW (1969) Chem Rev 69:365
5. Nagayama M, Tamura K (1968) Electrochim Acta 13:1773
6. Nagayama M, Tamura K (1967) Electrochim Acta 12:1097
7. Nagayama M, Tamura K, Takahashi H (1970) Corros Sci 10:617
8. Diggle JW (1973) Electrochim Acta 18:283
9. Diggle JW, Downie TC, Goulding CW (1970) Electrochim Acta 15:1079
10. Young L (1961) Anodic oxide films. Academic Press, London
11. Patermarakis G, Lenas P, Karavassilis Ch, Papayiannis G (1991) Electrochim Acta 36:709
12. Patermarakis G, Tzouvelekis D (1994) Electrochim Acta 39:2419
13. Leach SL, Neufeld F (1969) Corros Sci 9:225
14. Shreir LL (1976) Corrosion, vol. 2. Newnes-Butterworths, London
15. Smith AW (1973) J Electrochem Soc 120:1068
16. Kawai S, Ishiguro I (1976) J Electrochem Soc 123:1047
17. Rai K, Ruckenstein E (1975) J Catal 40:117
18. Chu Y, Ruckenstein E (1976) J Catal 41:384
19. Ihm SK, Ruckenstein E (1977) J Colloid Interface Sci 61:46
20. Ihm SK, Ruckenstein E (1978) Ind Eng Chem Prod Res Dev 17:110
21. Patermarakis G, Pavlidou C (1994) J Catal 147:140
22. Patermarakis G, Moussoutzanis K, Chandrinos J (1999) Appl Catal A 180:345
23. Patermarakis G, Nikolopoulos N (1999) J Catal 187:311
24. Fukuda Y, Fukushima T (1983) Electrochim Acta 28:47
25. Mason RB (1956) J Electrochem Soc 103:425
26. Tajima S, Umehara Y (1981) Plating Surf Finish 68:54
27. Tomita S (1981) Alutopia 11(4):15
28. Patermarakis G, Moussoutzanis K (2001) Corros Sci 43:1433
29. Patermarakis G, Moussoutzanis K (2001) Corros Sci (in press)
30. Patermarakis G, Moussoutzanis K (1995) Electrochim Acta 40:699
31. Patermarakis G (1998) J Electroanal Chem 447:25
32. O'Sullivan JP, Wood GC (1970) Proc R Soc (London) Ser A 317:511
33. Siejka J, Ortega C (1972) J Electrochem Soc 124:883
34. Neufeld P, Ali HO (1973) J Electrochem Soc 120:479
35. Ono S, Ichinose H, Masuko N (1991) J Electrochem Soc 138:3705
36. Patermarakis G, Moussoutzanis K (2001) J Electroanal Chem 510:59